Stereochemical plasticity modulates cooperative binding in a $Co^{II}_{12}L_6$ cuboctahedron

Felix J. Rizzuto, Jonathan R. Nitschke*

University of Cambridge, Department of Chemistry, Cambridge UK, CB2 1EW.

ABSTRACT: Biomolecular receptors are able to process information by responding differentially to combinations of chemical signals. Synthetic receptors that are likewise capable of multi-stimuli response can form the basis of programmable molecular systems, wherein specific input sequences create distinct outputs. Here we report a *pseud*o-cuboctahedral assembly capable of cooperatively binding anionic and neutral guest species. The binding of pairs of fullerene guests was observed to effect the all-or-nothing cooperative templation of an S_6-symmetric host stereoisomer. This bis-fullerene adduct exhibits different cooperativity in binding pairs of anions from the fullerene-free parent: In one case, positive cooperativity is observed, while in another all binding affinities are enhanced by an order of magnitude, and in a third the binding events are only minimally perturbed. This intricate modulation of binding affinity, and thus cooperativity, renders our new cuboctahedral receptor attractive for incorporation into systems with complex, programmable responses to different sets of stimuli.

Control over intermolecular interactions allows molecules to assemble into well-defined supramolecular structures that are able to achieve complex and varied functions.[1-11] A class of these materials, self-assembled metal-organic capsules are capable of binding small molecules,[12,13] catalysing reactions,[14-16] and responding to stimuli in well-defined ways.[17-19] Function in these capsules often results from the binding of a guest within a central void space. With a diverse range of capsular forms[20,21] that can manifest different stereochemistries,[22] the equally diverse range of cavities within this class of molecules enables the design of receptors for a wide range of guests.[23-25]

Engineering specific binding requires a complementary size and electrostatic relationship between host and guest.[26] As a result, large architectures capable of binding small substrates are rare. Closing off the interior void with bulky organic units,[27,28] using rigid ligands with cavity-directed substituents,[29] or exploiting unsaturated metal coordination sites,[30] are useful means of enforcing the binding of guests into discrete spaces.[31] However, these methods rely on pre-programmed features within the assembly. A more flexible approach would entail the preparation of a capsule capable of adapting its geometry,[32] altering the size of its cavity, the dimensions of its faces, the lengths of its edges or the areas of its apertures in response to guest binding events. Realising these structural reconfigurations would change the landscape for subsequent guests, bringing about cooperativity.

The conformational changes exhibited by biological receptors upon substrate binding exemplify this idea.[33] Both positive and negative cooperative binding, wherein the first binding event either improves or worsens the second,[34] respectively, are commonplace in these molecules. The ability of haemoglobin to cooperatively bind oxygen enhances its carrying capacity, whereas

the negative cooperative binding of glyceraldehyde-3-phosphate to the dehydrogenase GAPDH normalises the rate of sugar digestion.[35] The efficacy of these systems relies on small electronic or structural changes propagating through a system following the first binding event, regulating the affinity of the second binding. Translating cooperativity into complex supramolecular systems is a current challenge, as it relies on balancing dynamic rearrangement with structural integrity, and maintaining guest recognition upon geometric alteration.

RESULTS AND DISCUSSION

We hypothesised that a supramolecular system capable of both adapting to and regulating cooperative interactions could lead to a new means of control over the amplification of binding events.[36-39] We thus report a method for modulating the cooperativity of binding of a new $Co^{II}_{12}L_6$ assembly through the guest-mediated transformation of its stereochemistry. Upon binding C_{60} or C_{70}, the stereochemistry of the metal centres of our capsule was observed to reconfigure to optimise host-guest interactions, consequently influencing successive binding events at the triangular apertures of the cage (Figure 1). When no guests were centrally bound, *O*-symmetric architecture **1** displayed a negative cooperative interaction with icosahedral anionic guests. Following the binding of two fullerenes, host **1** was observed to transform into its S_6-symmetric isomer, **2**, which displayed positive cooperativity during the binding of two $B_{12}F_{12}^{2-}$ guests, in contrast to **1**. Stereochemical transformations within this system thus led to the regulation of long range interactions between guests, modulating the specific modes and degrees of cooperativity (either positive or negative) expressed around the periphery of the cages.

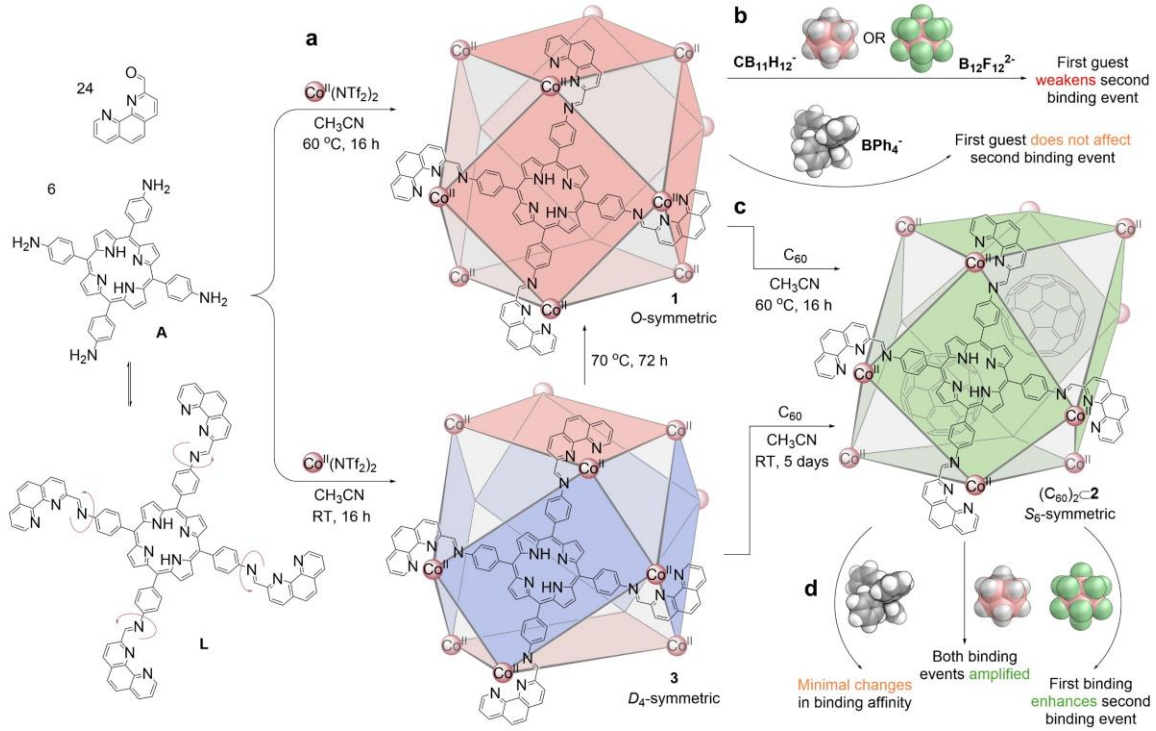

Figure 1 | Syntheses of the $Co^{II}_{12}L_6$ isomers 1-3 and their responses to the binding of large anionic guests. a, *O*-symmetric **1** (pink faces represent ligands on C_4 symmetry axes) and D_4-symmetric **3** (blue faces depict ligands on C_2 symmetry axes). **b,** In **1**, icosahedral anionic guests repel each other, leading to negative cooperativity. **c,** The addition of C_{60} to either **1** or **3** leads to the generation of the S_6-symmetric framework of **2** (green faces depict the ligands, which do not lie on symmetry axes). **d,** $(C_{60})_2\subset$**2** binds the same anions as **1**, but with dramatically altered cooperativities and affinities.

Synthesis and characterisation of 1

The self-assembly of free base tetrakis(*p*-aminophenyl)porphyrin **A** (6 equiv) and 2-formylphenanthroline (24 equiv) subcomponents with cobalt(II) trifluoromethanesulfonimide (triflimide, NTf_2^-) (12 equiv) was observed by ESI-MS (Supplementary Fig. 2) to produce $Co^{II}_{12}L_6$ cage **1**, following heating at 60 °C overnight in CH_3CN (Supplementary Section 2). The wide-sweep ^1H NMR spectrum indicated that the product was highly symmetric; dispersion of the thirteen proton signals of the ligand over the range 240 to –20 ppm confirmed their coordination to paramagnetic Co^{II} centres with maintenance of fourfold ligand symmetry. Even when 30% excess of Co^{II} was used, no metalation of the free base porphyrin was observed during the assembly process.

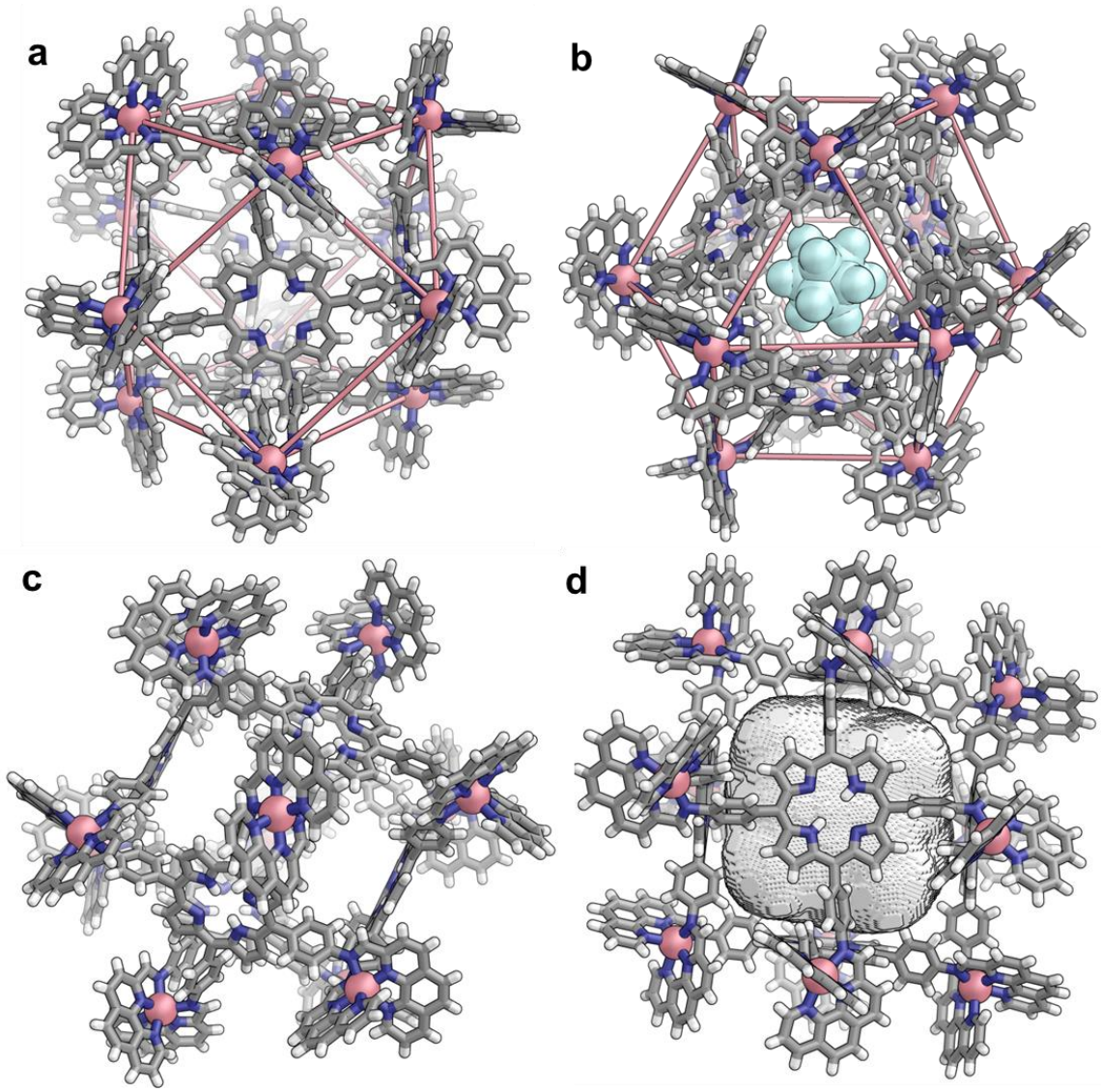

Figure 2 | X-ray crystal structure of 1. a & b, Two views showing the cuboctahedral framework of Co^{II} ions of **1** (highlighted with solid pink lines), with **b** additionally depicting one of three $CB_{11}H_{12}^-$ anions localised in a triangular pocket of **1**. **c,** Side-on view depicting the bis-tridentate coordination environment around the Co^{II} ions. **d,** Viewed down a fourfold symmetry axis perpendicular to a square face. The central void is highlighted as a light gray solid. Solvent and anions are removed for clarity (Co^{II}, pink; C, grey; N, blue; H, white, $CB_{11}H_{12}^-$, cyan).

Slow diffusion of $^iPr_2O$ into a solution of **1** containing $CsCB_{11}H_{12}$ (12 equiv) in CH_3CN provided X-ray quality crystals suitable for diffraction analysis (Figure 2). The cationic portion of

the crystal structure revealed a cuboctahedral arrangement of Co^{II} ions, presenting six square faces occupied by ligands and eight triangular apertures between ligands. All metal centres within a structure have the same Δ or Λ handedness. Both enantiomers of **1** are observed in the crystal. The architecture has approximate *O* (chiral octahedral) point symmetry, consistent with its ^{1}H NMR spectrum, and encloses an interior cavity of 2888 $Å^3$, calculated using VOIDOO[40] (Figure 2d). The chelation planes[41] of the two imino-phenanthroline moieties bound to each Co^{II} centre intersect at an angle of 79-84°. Adjacent Co^{II}–Co^{II} distances average 14.7 Å and antipodal metal centres are separated by *ca.* 30.0 Å. This work builds upon reports of *edge-linked* Archimedean solids by the groups of Ward[42], Stang[43] and Fujita[44], to construct the first *face-capped* cuboctahedral structure, enabling an unprecedented enclosure of the central cavity of **1**.

Cooperative templation of 2

Host-guest investigations revealed that **1** bound fullerenes with high affinity. The addition of the acetonitrile-insoluble fullerenes C_{60}, C_{70} or [6,6]-phenyl C_{61} butyric acid methyl ester (PCBM) (*ca.* 5 equiv each, excess) to a solution of **1** led to significant changes in the wide-sweep ^{1}H NMR spectra after heating at 60 °C for 16 h. In all cases approximately four times the original number of signals were observed (Figure 3b). ESI-MS revealed the presence of an adduct of two fullerenes in all cases (Figure 3a). In order to probe the stability of the singly occupied host-guest complex, 1.5 equivalents of C_{60} were added to a CD_3CN solution of **1** and heated to 60 °C for 16 h. Both ^{1}H NMR and ESI-MS showed only peaks corresponding to the free cage and the doubly-occupied host-guest species; no singly occupied species could be identified (Supplementary Fig. 16 and 17). This experiment reflects all-or-nothing cooperative binding of fullerenes within the cavity of the assembly.

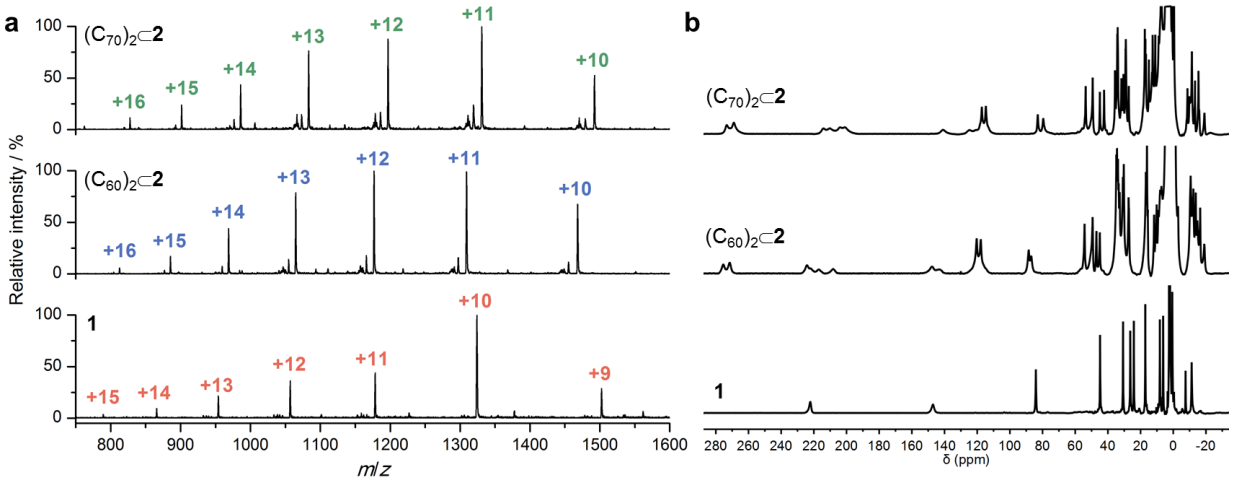

Figure 3 | Characterisation data for 1, $(C_{60})_2$⊂2 and $(C_{70})_2$⊂2. a, ESI mass spectra and **b,** wide sweep ^{1}H NMR spectra (400 MHz, 298 K, CD_3CN). The data indicate fourfold desymmetrisation of the proton environments in **2** with maintenance of $Co^{II}_{12}L_6$ stoichiometry.

Single crystal X-ray diffraction analysis unambiguously revealed that C_{60} induced a significant stereochemical alteration to **1**, generating isomer **2** (Figure 4). Unexpectedly, the vertices of $(C_{60})_2$⊂**2** were not all of the same handedness – both Δ- and Λ-handed metal centres were present in a 1:1 ratio. On each ligand, one set of transverse branches was *syn*, while the other was *anti*,

resulting in overall C_1 symmetry of the ligands. This is consistent with the ^{1}H NMR data (Figure 3b), which suggests complete desymmetrisation of the ligand environments in $(C_{60})_2\subset$**2**.

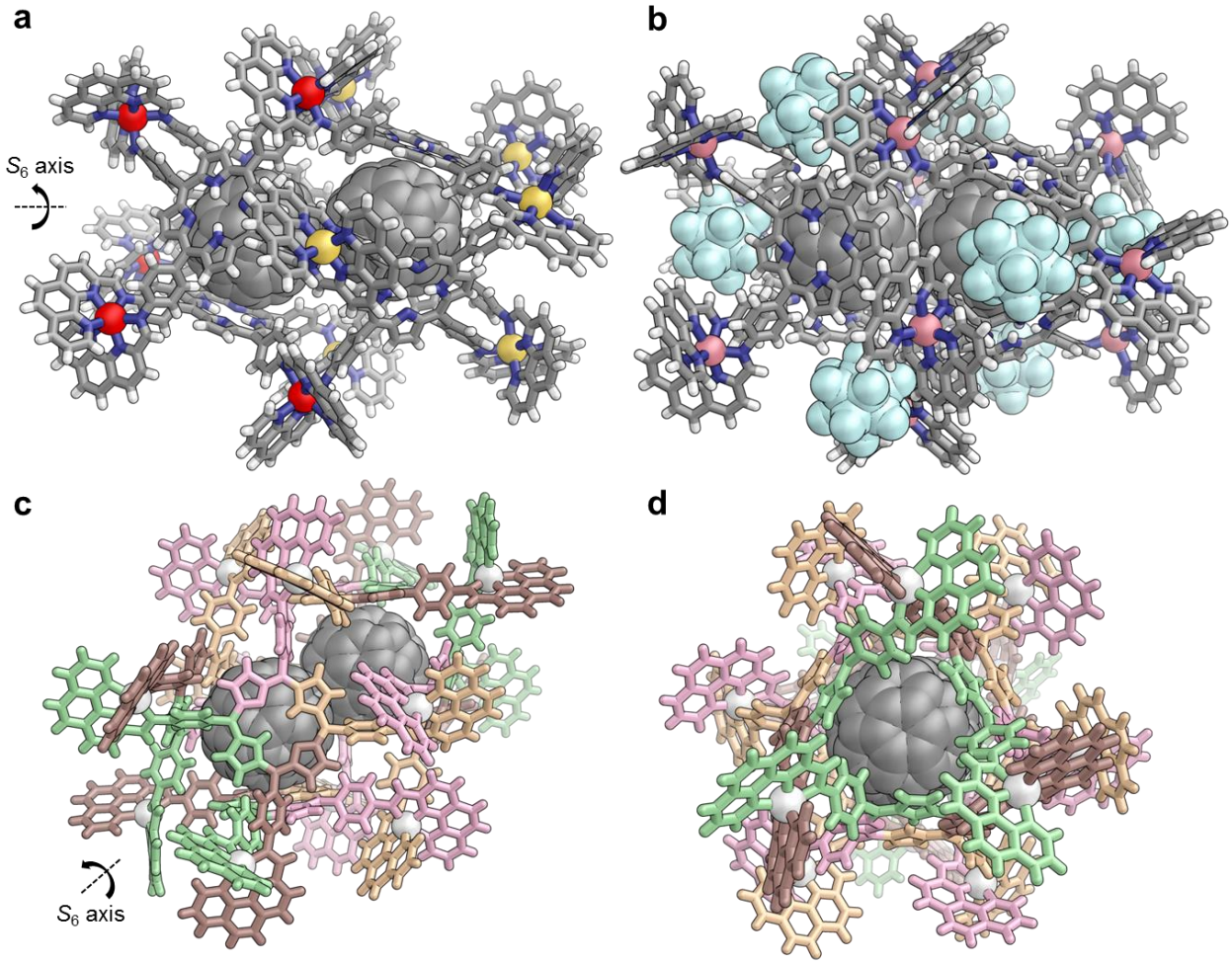

Figure 4 | Four views of the X-ray crystal structure of $(C_{60})_2\subset$2. a, Λ metal centres are coloured red and Δ centres are coloured yellow. **b,** Shown with the $CB_{11}H_{12}^-$ anions that are localised at the triangular apertures of the architecture. **c,** View perpendicular to a ligand face, and **d,** view down the S_6 axis, where each colour represents a different ligand environment and Co^{II} is coloured white.

Structurally, this reconfiguration results in a compression of the metal-metal distances along the equatorial belt, accompanied by a lengthening of the shortest distances between axial and equatorial metal centres. Adjacent Co^{II}–Co^{II} vectors thus generate six irregular quadrilateral faces, occupied by ligands. The apertures of the structure comprise two equilateral triangles at the axial ends, orthogonal to the S_6 axis of the cage, and six approximately right-angled triangles around the equator, maintaining the cuboctahedral connectivity of the assembly. The degree of strain around the Co^{II} ions was inferred to be larger than in **1**, with the angles between chelation planes in the range 74-89°. The S_6 point symmetry of **2** renders it achiral, with each metal centre of Δ handedness related by inversion to a metal centre of Λ handedness (Figure 4a).

The axial elongation and stereochemical reconfiguration of **1** to generate **2** thus maximises contacts both between fullerenes and between the host and guests. The rearrangement required in order to bind the first fullerene leads to the formation of a configuration better able to bind the second, leading to cooperativity.

Adding equimolar amounts of C_{60} and C_{70} concurrently to **1** led to a statistical mixture of fullerene adducts of **2**. Each of $(C_{60})_2\subset$**2**, $C_{60}C_{70}\subset$**2** and $(C_{70})_2\subset$**2** were observed by ESI-MS (Supplementary Fig. 15) and ^{1}H NMR spectroscopy (Supplementary Fig. 13 and 14). Integration of the ^{1}H NMR spectrum (Supplementary Fig. 13) indicated that $(C_{70})_2\subset$**2** was slightly more abundant than $C_{60}C_{70}\subset$**2**, and that both of these were more abundant than $(C_{60})_2\subset$**2** (the ratio of $(C_{60})_2\subset$**2**:$C_{60}C_{70}\subset$**2**:$(C_{70})_2\subset$**2** was *ca.* 2:9:10). The similarity of the proton spectra between each fullerene-occupied species (Supplementary Fig. 8) suggests that all three fullerenes induce the same stereochemical change from **1** to **2**. We were unable to follow the rate of conversion from **1** to **2** due to the lack of stability of **1** in any solvent capable of dissolving fullerenes.

Regulation of cooperative binding events

Further host-guest investigations revealed the propensity of **1** to bind large anionic guests (Supplementary Section 6). While both carborate ($CB_{11}H_{12}^-$) and tetraphenylborate (BPh_4^-) anions were observed to bind in fast exchange with **1** by ^{1}H NMR, the rate of exchange of $B_{12}F_{12}^{2-}$ with **1** was slower, approximating intermediate exchange on the NMR timescale. A sample of **1** containing $B_{12}F_{12}^{2-}$ (5 equiv) gave a single ^{19}F signal distinct from the chemical shift of free $B_{12}F_{12}^{2-}$, verifying binding to **1** (Supplementary Fig. 29). For both $CB_{11}H_{12}^-$ and BPh_4^-, the proton signals of the guest were observed to shift downfield by 1-4 ppm, relative to their unbound states, after binding to **1** (Supplementary Fig. 19 and 23).

Affinity constants for $CB_{11}H_{12}^-$ and BPh_4^- were determined by ^{1}H NMR titrations, while the affinity of $B_{12}F_{12}^{2-}$ was determined by UV-Vis titration. All anions produced sigmoidal residuals when fitted to a 1:1 binding isotherm (Supplementary Fig. 20 and 24). When instead fitted to 1:2 binding isotherms, only random residuals were observed, indicating two distinct binding events to **1** (Supplementary Fig. 21, 25 and 31). In all cases, the affinity constants for the first and second bindings (K_1 and K_2, respectively) were determined from a global shift analysis of the titration data using Bindfit[45,46]; the results were averaged over two runs (Table S2). The cooperativity was quantified using the allosteric cooperativity factor α (where $\alpha = 4K_2/K_1$: $\alpha > 1$ indicates positive cooperativity, $\alpha < 1$ indicates negative cooperativity, and $\alpha = 1$ indicates non-cooperative binding). Both $CB_{11}H_{12}^-$ and $B_{12}F_{12}^{2-}$ displayed negative cooperative binding to **1**, while BPh_4^- was observed to approximate non-cooperative behaviour. These data are displayed in Table 1 and depicted graphically in Figure 5.

Guest localisations were inferred by considering the crystallographic and titration data together. In **1**, we propose that guests are localised around the eight triangular apertures of the architecture, given that three of the twelve resolved carborate anions are nestled within the triangular apertures of the architecture (Figure 2b), and that the most significant proton shifts were observed for the most downfield-shifted protons (that is, those closest to the Co^{II} centres) for all guest titrations (Supplementary Fig. 19, 23 and 27). However, solid-state guest localisations do not necessarily reflect binding stoichiometries in solution.[47] As a 1:2 host:guest isotherm represents the simplest model to adequately fit the titration data, we infer that rapid exchange of the guests between the triangular sites serves to prevent the observation of higher binding stoichiometries in solution.

Table 1 | Summary of the binding constants (K_1 and K_2, M^{-1}) of anionic guests with capsule **1**, $(C_{60})_2$⊂**2** and $(C_{70})_2$⊂**2**.

Guest		**1**	$(C_{60})_2$⊂**2**	$(C_{70})_2$⊂**2**
BPh_4^-	K_1	$1.86 \pm 0.02 \times 10^3$	$2.63 \pm 0.03 \times 10^3$	$2.43 \pm 0.03 \times 10^3$
	K_2	$5.9 \pm 0.1 \times 10^2$	$6.56 \pm 0.02 \times 10^2$	$3.5 \pm 0.1 \times 10^2$
	α	1.3 ± 0.1	1.00 ± 0.01*	0.58 ± 0.02
$CB_{11}H_{12}^-$	K_1	$2.61 \pm 0.02 \times 10^3$	$1.1 \pm 0.1 \times 10^4$	$1.0 \pm 0.1 \times 10^4$
	K_2	$1.7 \pm 0.2 \times 10^2$	$1.56 \pm 0.05 \times 10^3$	$1.3 \pm 0.1 \times 10^2$
	α	0.26 ± 0.03	0.57 ± 0.05	0.052 ± 0.007
$B_{12}F_{12}^{2-}$	K_1	$1.5 \pm 0.1 \times 10^6$	$1.5 \pm 0.1 \times 10^3$	$2.2 \pm 0.1 \times 10^4$
	K_2	$1.89 \pm 0.02 \times 10^4$	$1.4 \pm 0.1 \times 10^4$	$3.2 \pm 0.1 \times 10^3$
	α	0.050 ± 0.003	37 ± 4	0.58 ± 0.03

* Regression was restrained to approximate non-cooperative behaviour ($K_1 = 4K_2$).

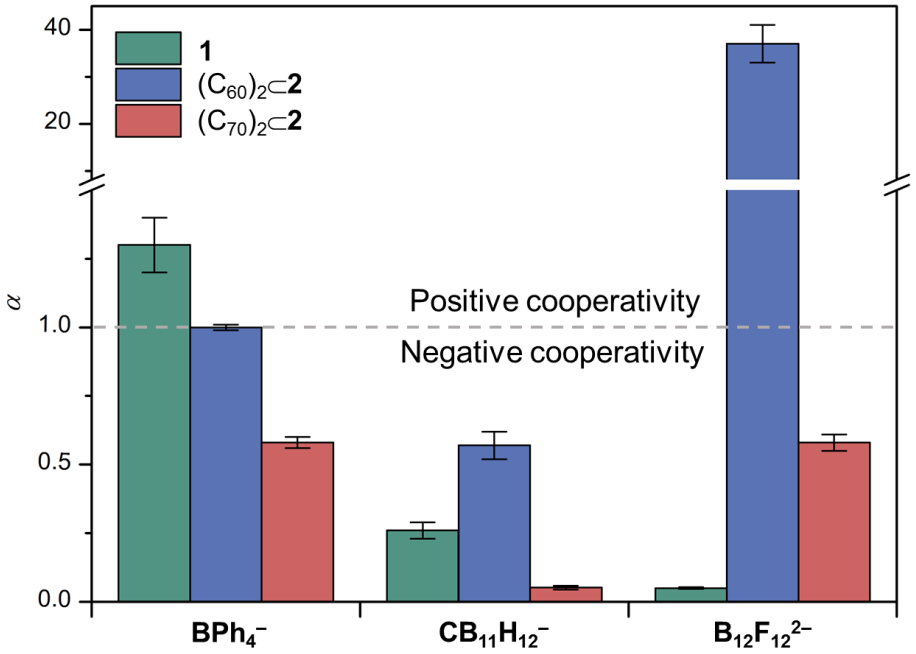

Figure 5 | The changes observed in the cooperativity parameter ($\alpha = 4K_2/K_1$) when fullerenes were present in the cage. The dashed line represents the border between positive and negative cooperative binding. Values are reported as weighted averages of two titrations; asymptotic errors are calculated at the 95% Confidence Interval level.

The dispersion of the fifty-two unique proton signals of $(C_{60})_2$⊂**2** and $(C_{70})_2$⊂**2** over their wide-sweep ^{1}H NMR spectra enabled the binding affinities of $CB_{11}H_{12}^-$, BPh_4^- and $B_{12}F_{12}^{2-}$ to be quantified by global proton shift analysis.[45] All anionic guests induced distinct proton shifts throughout their titration, consistent with fast exchange binding on the NMR timescale (Supplementary Section 7). As with **1**, a 1:2 binding model best fit the titration data. The affinity of BPh_4^- showed little difference between assemblies; however, $CB_{11}H_{12}^-$ binding was enhanced, and $B_{12}F_{12}^{2-}$ decreased, when fullerenes were present in the cage (Table 1). In the case of $CB_{11}H_{12}^-$, K_1 increased fourfold in $(C_{60})_2$⊂**2** and $(C_{70})_2$⊂**2**, as compared to **1**; K_2 was nine times larger in $(C_{60})_2$⊂**2** than in $(C_{70})_2$⊂**2** or **1**. When binding $B_{12}F_{12}^{2-}$, K_1 decreased by three orders of

magnitude in $(C_{60})_2\subset$**2** and two orders of magnitude in $(C_{70})_2\subset$**2**, from the baseline of **1**. Furthermore, whereas most anions exhibited negative cooperative binding to $(C_{60})_2\subset$**2** and $(C_{70})_2\subset$**2**, $B_{12}F_{12}^{2-}$ was observed to bind to $(C_{60})_2\subset$**2** with positive cooperativity (Figure 5). A decrease in the kinetic uptake ratio k_{in}/k_{out} of the binding of $B_{12}F_{12}^{2-}$ was also observed when going from **1** to $(C_{60})_2\subset$**2**, as reflected in the transition from intermediate to fast exchange binding of $B_{12}F_{12}^{2-}$ on the NMR timescale (Supplementary Fig. 42 and 54).

The regulation of binding events observed for $(C_{60})_2\subset$**2** and $(C_{70})_2\subset$**2**, compared to **1**, is surprising given that the central voids of $(C_{60})_2\subset$**2** and $(C_{70})_2\subset$**2** are too small to accommodate guests of this size. Two explanations appear plausible: firstly, the cage framework may be flexible enough to expand and accommodate guests, or secondly, binding may occur on the exterior of the structure. All twenty-four carborate anions were resolved in the crystal structure of $(C_{60})_2\subset$**2**, none of which are located in the cavity of the assembly. However, a carborate anion was observed around every aperture: two cap the axial apertures along the S_6 axis, at opposite ends of the cage, and six sit in the triangular pockets ringing its equator (Figure 4b). Guests thus appear to associate with the exterior pockets, rather than interior cavity, of the cage.

Among all anionic guests, the presence of C_{60} produced higher K_2 and α values than the presence of C_{70} (Table 1 and Figure 5). This indicates that the inclusion of C_{70} enforces a stronger negative cooperative interaction than C_{60} in **2**. We initially ascribed the variances in cooperativity to the different electronic properties of the fullerene guests (acceptors) interacting with porphyrin units (donors).[48] Although the UV-Vis spectra of all fullerene-bound complexes revealed red shifts in the Soret (+7 nm) and Q bands (*ca.* +5 nm) of the porphyrin units compared to **1**, the contraction of the HOMO/LUMO gap appeared uniform across all host-guest complexes (Supplementary Fig. 12).

We thus hypothesise that the observed differences in cooperativity instead resulted from the dissimilarities in sphericity and aperture-blocking character engendered by the two fullerenes. Upon binding, both fullerenes are expected to exhibit a δ^- polarisation close to the Co^{II} cations, resulting in a balancing δ^+ polarisation pointing inwards to the cavity. As elliptical C_{70} is larger than spherical C_{60}, the fullerene surface area adjacent to the apertures will be larger in $(C_{70})_2\subset$**2** than in $(C_{60})_2\subset$**2**. A greater surface area of δ^- polarisation will therefore occur near the apertures of $(C_{70})_2\subset$**2** compared to $(C_{60})_2\subset$**2**, potentially increasing the degree of charge repulsion experienced by anionic guests around the apertures of the cage. Slight structural differences between the cages in accommodating fullerenes of different sizes may also be a contributing factor to the observed differences in guest binding strengths. Attempts to study the host-guest chemistry of a fullerene-free Co^{III} congener of **2** by an 'assembly-followed-by-fixing' approach[49] proved unsuccessful (Supplementary Section 5.1).

Further stereochemical diversity

The stereochemical plasticity of **L**, exhibited in the distinct geometries of both **1** and **2**, prompted us to investigate whether the same set of subcomponents and Co^{II} might form other diastereomers without templation. The same building blocks that formed **1** (after 16 h at 60 °C in CD_3CN) were observed to form another species when stirred in CD_3CN at room temperature overnight. The wide sweep ^1H NMR spectrum (Supplementary Fig. 59) of this new species exhibited a series of broader, shifted peaks. Intriguingly, the ESI mass spectrum of this mixture

corresponded to a $Co^{II}_{12}L_6$ species (Supplementary Fig. 60), despite the absence of signals attributable to **1** by ^{1}H NMR spectroscopy.

The subsequent diffusion of Et_2O into this solution (containing approximately 20 equivalents of Bu_4NBF_4) yielded single crystals of **3** (Figure 6). X-ray diffraction revealed a similar cuboctahedral metal connectivity as **1** and **2**, however, the assembly displayed D_4 symmetry: four ligands on twofold symmetry axes span the equatorial plane of the structure, and two ligands, each with fourfold rotational symmetry, cap the axial positions (Figure 6b). The structure thus presents a mixture of square and rectangular ligand-occupied faces with scalene triangular apertures, as opposed to the square faces and equilateral triangular apertures of **1** (Figure 1).

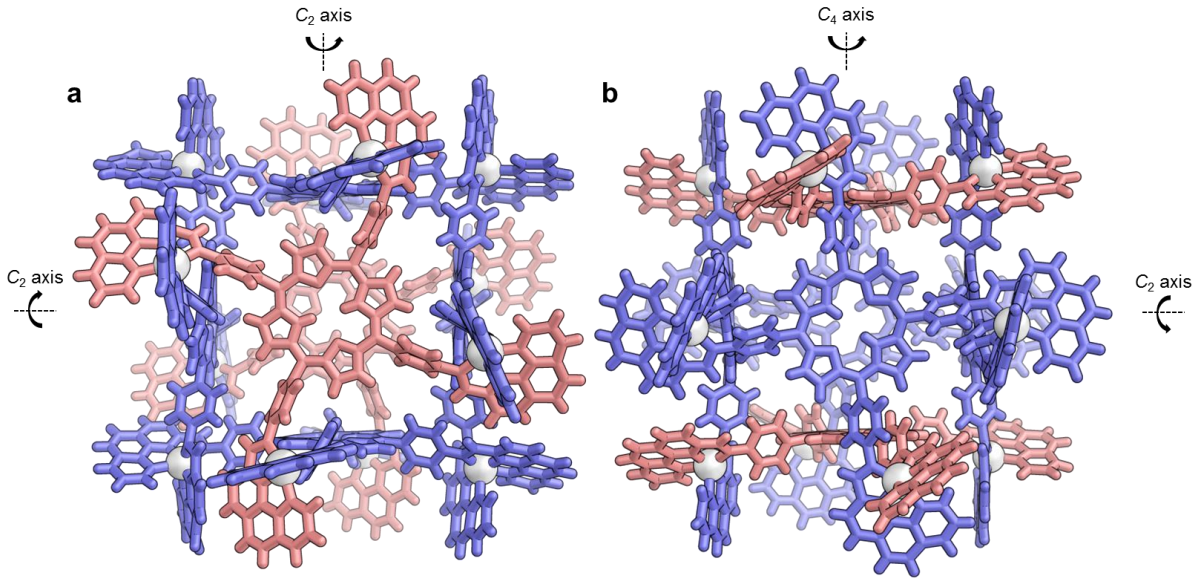

Figure 6 | Two views of the X-ray crystal structure of *D*$_4$-symmetric 3. a, Perpendicular to a fourfold-symmetric ligand (pink). **b,** Perpendicular to a twofold-symmetric ligand (blue) (Co^{II}, white).

The chiral structure contains a 1:2 ratio of Δ and Λ metal nodes. Both enantiomers are present in the crystal. The angles between the chelation planes of the imino-phenanthroline moieties are in a similar range (79-85°) to those of **1**, indicating that there is little coordinative strain difference between the two structures.

Despite its broad ^{1}H NMR spectrum, travelling wave ion mobility ESI mass spectra of **3** revealed only a single drift time for each signal corresponding to an $Co^{II}_{12}L_6$ architecture (Supplementary Fig. 61), suggesting that **3** is the principal product in solution. When **3** was heated to 50 °C for a further 24 hours, the ^{1}H NMR signals of **1** were observed to grow into the spectrum (Supplementary Fig. 59). *O*-symmetric cage **1** was observed by ^{1}H NMR spectroscopy to predominate after heating the mixture to 70°C for 72 hours. Likewise, the addition of C_{60} or C_{70} to **3** generated $(C_{60})_2$⊂**2** and $(C_{70})_2$⊂**2** after stirring at room temperature for five days.

Conclusion

A molecular scaffold was developed that can alter its geometry without altering its stoichiometry, providing a new platform for understanding flexible and adaptable chemical systems. The ability of **1** to exhibit three distinct isomeric forms, converting from a *D*$_4$- to *O*- to

S_6-symmetric architecture, is unprecedented for a supramolecular entity of its size. Using cooperative templation by fullerene guests, the stereochemistry of the capsule can be altered. This leads to a change in cage morphology without altering the connectivity of the framework, resulting in the regulation of cooperative intermolecular interactions. Our study provides a novel method for both tuning the strength of guest binding and optimising the system to exhibit specific modes of cooperativity.

Acknowledgements

This work was supported by the UK Engineering and Physical Sciences Research Council (EPSRC). F.J.R. acknowledges Cambridge Australia Scholarships and the Cambridge Trust for PhD funding. We thank Diamond Light Source for time on Beamline I19 (MT11397). We also thank Tanya Ronson for helpful discussions regarding crystallography, and Marion Kieffer and John Carpenter for assisting with synchrotron X-ray data collections.

Author contributions

J.R.N. and F.J.R. conceived the study, analysed the results and wrote the manuscript. F.J.R. performed the experiments.

Competing financial interests

The authors declare no competing financial interests.

Methods

Synthesis of 1. Free base tetrakis(*p*-aminophenyl)porphyrin **A** (41.5 mg, 60.0 μmol, 6 equiv.), $Co(NTf_2)_2{\cdot}6H_2O$ (87.4 mg, 120 μmol, 12 equiv.) and 2-formylphenanthroline (50.0 mg, 240 μmol, 24 equiv.) were stirred in CD_3CN (5.00 mL) at 60 °C for 16 h in a sealed vessel, yielding a dark orange stock solution upon cooling (2.00 mM). Standard solutions of 0.200 mM (0.050 mL of stock solution made up to 0.500 mL) were used for ^{1}H NMR titrations. ^{1}H NMR (400 MHz, 298 K, CD_3CN): δ 222.2, 147.1, 84.1, 44.8, 30.8, 26.3, 24.1, 17.1, 8.2, 6.2, 0.6, –7.5, –11.3 ppm. ^{19}F NMR (376 MHz, 298 K, CD_3CN): δ –79.1 ppm. ESI-MS [charge fragment]: *m/z* = 1501.3 [**1**$(NTf_2)_{15}^{9+}$], 1323.5 [**1**$(NTf_2)_{14}^{10+}$], 1177.5 [**1**$(NTf_2)_{13}^{11+}$], 1056.4 [**1**$(NTf_2)_{12}^{12+}$], 953.3 [**1**$(NTf_2)_{11}^{13+}$], 865.2 [**1**$(NTf_2)_{10}^{14+}$], 789.2 [**1**$(NTf_2)_9^{15+}$]. X-ray quality crystals were grown from the slow diffusion of *i*Pr_2O into a solution of **1** containing $CsCB_{11}H_{12}$ (*ca.* 12 equivalents) in CD_3CN (Supplementary Section 3.1).

Syntheses of host-guest complexes of 2. To a solution of **1** (2.00 mM in CD_3CN, 1 mL) was added C_{60} (13 mg, 5 equiv) or C_{70} (15 mg, 5 equiv) directly. PCBM (7 mg, 5 equiv.) was added to a sample of **1** (0.5 mL, 1.00 mM in CD_3CN). The mixtures were sonicated for 10 minutes, then stirred at 60 °C for 16 h in a sealed vessel. Upon cooling, the mixture was centrifuged. The supernatant was collected and used without further purification (concentration = 2.00 mM). For subsequent NMR titrations, 0.05 mL of these solutions was made up to 0.5 mL with CD_3CN, yielding 0.200 mM stock solutions. In all cases, the paramagnetic nature of the complexes hampered complete signal assignment.

$(C_{60})_2\subset$**2**. ^{1}H NMR (400 MHz, 298 K, CD_3CN): δ 275.4, 271.5, 224.3, 223.0, 217.1, 208.5, 147.7, 142.8, 120.4, 117.8, 88.5, 87.0, 54.3, 49.3, 47.0, 45.0, 34.8, 34.4, 33.9, 33.4, 32.8, 30.8, 30.3, 27.3, 27.1, 16.8, 16.1, 15.6, 11.7,

10.7, 10.2, 9.1, 8.0, 7.2, –0.9, –2.9, –10.6, –12.4, –13.8, –14.8, –16.5, –19.0 ppm. ESI-MS [charge fragment]: *m/z* = 1468.2 [**2**$(C_{60})_2(NTf_2)_{14}^{10+}$], 1309.3 [**2**$(C_{60})_2(NTf_2)_{13}^{11+}$], 1176.8 [**2**$(C_{60})_2(NTf_2)_{12}^{12+}$], 1064.9 [**2**$(C_{60})_2(NTf_2)_{11}^{13+}$], 968.8 [**2**$(C_{60})_2(NTf_2)_{10}^{14+}$], 885.6 [**2**$(C_{60})_2(NTf_2)_9^{15+}$], 812.7 [**1**$(C_{60})_2(NTf_2)_8^{16+}$]. X-ray quality crystals were grown from the slow diffusion of Et_2O into a solution of $(C_{60})_2$⊂**2** containing $CsCB_{11}H_{12}$ (*ca.* 30 equivalents) in CD_3CN (Supplementary Section 3.2).

$(C_{70})_2$⊂**2**. ^{1}H NMR (400 MHz, 298 K, CD_3CN): δ 273.3, 268.9, 214.2, 210.4, 204.1, 200.9, 141.0, 124.8, 117.2, 114.7, 83.0, 79.6, 53.6, 49.3, 44.9, 42.3, 35.7, 34.3, 34.1, 33.9, 31.8, 30.5, 29.2, 29.0, 27.3, 17.4, 17.1, 16.7, 15.0, 13.1, 12.6, 11.0, 8.9, 7.5, 7.2, 5.0, 0.6, –0.4, –8.7, –9.9, –10.9, –11.4, –13.3, –15.4, –15.9, –19.1 ppm. ESI-MS [charge fragment]: *m/z* = 1492.3 [**2**$(C_{70})_2(NTf_2)_{14}^{10+}$], 1331.1 [**2**$(C_{70})_2(NTf_2)_{13}^{11+}$], 1196.8 [**2**$(C_{70})_2(NTf_2)_{12}^{12+}$], 1083.3 [**2**$(C_{70})_2(NTf_2)_{11}^{13+}$], 985.9 [**2**$(C_{70})_2(NTf_2)_{10}^{14+}$], 901.5 [**2**$(C_{70})_2(NTf_2)_9^{15+}$], 827.7 [**2**$(C_{70})_2(NTf_2)_8^{16+}$].

$(PCBM)_2$⊂**2**. ^{1}H NMR (400 MHz, 298 K, CD_3CN): δ 275.3, 270.9, 227–195 (broad) 119.5, 117.7, 54.0, 50.1, 49.4, 34.5, 34.0, 30.7, 29.6, 26.7, 17.4, 16.7, 16.2, 11.7, 10.5, 10.2, 9.3, 9.0, 8.3, 7.8, 5.6, 3.5, 0.3, –1.7, –2.2, –2.9, –4.4, –4.9, –6.8, –7.0, –7.3, –10.9, –12.5, –13.9, –15.2, –16.3, –19.2 ppm. ESI-MS [charge fragment]: *m/z* = 1506.3 [**2**$(C_{72}H_{14}O_2)_2(NTf_2)_{14}^{10+}$], 1343.8 [**2**$(C_{72}H_{14}O_2)_2(NTf_2)_{13}^{11+}$], 1208.6 [**2**$(C_{72}H_{14}O_2)_2(NTf_2)_{12}^{12+}$], 1094.1 [**2**$(C_{72}H_{14}O_2)_2(NTf_2)_{11}^{13+}$], 996.0 [**2**$(C_{72}H_{14}O_2)_2(NTf_2)_{10}^{14+}$], 911.0 [**2**$(C_{72}H_{14}O_2)_2(NTf_2)_9^{15+}$], 836.6 [**2**$(C_{72}H_{14}O_2)_2(NTf_2)_8^{16+}$].

Synthesis of 3. Free base tetrakis(*p*-aminophenyl)porphyrin **A** (2.49 mg, 3.60 μmol, 6 equiv.), $Co(NTf_2)_2{\cdot}6H_2O$ (5.24 mg, 7.20 μmol, 12 equiv.) and 2-formylphenanthroline (3.00 mg, 14.4 μmol, 24 equiv.) were stirred in CD_3CN (0.5 mL) at room temperature for 16 h in a sealed NMR tube. The solution was cooled to room temperature to yield a dark orange solution. ^{1}H NMR (400 MHz, 298 K, CD_3CN): δ 274–260 (broad), 228–210 (broad), 118.3, 49.8, 49.5, 47.4, 30.7, 24.6, 16.7, 15.3, 14.4, 8.5, 7.5, –0.6, –5.5, –9.6, –13.4, –14.2, –17.2 ppm. The broad paramagnetic signals hampered further peak identification. ESI-MS: as **1**. X-ray quality crystals were grown from the slow diffusion of Et_2O into a solution of **3** containing Bu_4NBF_4 (*ca.* 20 equivalents) in CD_3CN (Supplementary Section 3.3).

Crystallographic data for the structures reported in this paper have been deposited at the Cambridge Crystallographic Data Center, under the deposition numbers 1510849 (**1**), 1510850 ($(C_{60})_2$⊂**2**), and 1510851 (**3**). Copies of these data can be obtained free of charge via www.ccdc.cam.ac.uk/data_request/cif. All other data supporting the findings of this study are available within the article and its Supplementary Information files, or from the corresponding author upon reasonable request**.**

References

1. Stupp, S. I., Palmer, L. C. Supramolecular chemistry and self-assembly in organic materials design. *Chem. Mater.* **26**, 507-518 (2014).
2. Aliprandi, A., Mauro, M., De Cola, L. Controlling and imaging biomimetic self-assembly. *Nat. Chem.* **8**, 10-15 (2016).
3. Zhao, H., *et al.* Reversible trapping and reaction acceleration within dynamically self-assembling nanoflasks. *Nat. Nano.* **11**, 82-88 (2016).
4. Lee, S., Chen, C.-H., Flood, A. H. A pentagonal cyanostar macrocycle with cyanostilbene CH donors binds anions and forms dialkylphosphate [3]rotaxanes. *Nat. Chem.* **5**, 704-710 (2013).
5. Mitra, T., *et al.* Molecular shape sorting using molecular organic cages. *Nat. Chem.* **5**, 276-281 (2013).
6. Krieg, E., Weissman, H., Shirman, E., Shimoni, E., Rybtchinski, B. A recyclable supramolecular membrane for size-selective separation of nanoparticles. *Nat. Nano.* **6**, 141-146 (2011).
7. Zhang, Z., *et al.* Expanded porphyrin-anion supramolecular assemblies: environmentally responsive sensors for organic solvents and anions. *J. Am. Chem. Soc.* **137**, 7769-7774 (2015).

8. Shopsowitz, K. E., Qi, H., Hamad, W. Y., MacLachlan, M. J. Free-standing mesoporous silica films with tunable chiral nematic structures. *Nature* **468**, 422-425 (2010).
9. Sadownik, J. W., Mattia, E., Nowak, P., Otto, S. Diversification of self-replicating molecules. *Nat. Chem.* **8**, 264-269 (2016).
10. Miller, R. G., Brooker, S. Spin crossover, reversible redox, and supramolecular interactions in 3*d* complexes of 4-(4-pyridyl)-2,5-dipyrazyl-pyridine. *Inorg. Chem.* **54**, 5398-5409 (2015).
11. Cha, W.-Y., *et al.* Multifaceted [36]octaphyrin(1.1.1.1.1.1.1.1): deprotonation-induced switching among nonaromatic, Mobius aromatic, and Huckel antiaromatic species. *Chem. Commun.* **52**, 6076-6078 (2016).
12. Schmuck, C. Guest encapsulation within self-assembled molecular containers. *Angew. Chem. Int. Ed.* **46**, 5830-5833 (2007).
13. Sato, H., *et al.* Positive heterotropic cooperativity for selective guest binding via electronic communications through a fused zinc porphyrin array. *J. Am. Chem. Soc.* **127**, 13086-13087 (2005).
14. Brown, C. J., Toste, F. D., Bergman, R. G., Raymond, K. N. Supramolecular catalysis in metal–ligand cluster hosts. *Chem. Rev.* **115**, 3012-3035 (2015).
15. Cullen, W., Misuraca, M. C., Hunter, C. A., Williams, N. H., Ward, M. D. Highly efficient catalysis of the Kemp elimination in the cavity of a cubic coordination cage. *Nat. Chem.* **8**, 231-236 (2016).
16. Wang, Z. J., Clary, K. N., Bergman, R. G., Raymond, K. N., Toste, F. D. A supramolecular approach to combining enzymatic and transition metal catalysis. *Nat. Chem.* **5**, 100-103 (2013).
17. McConnell, A. J., Wood, C. S., Neelakandan, P. P., Nitschke, J. R. Stimuli-responsive metal–ligand assemblies. *Chem. Rev.* **115**, 7729-7793 (2015).
18. Carnes, M. E., Collins, M. S., Johnson, D. W. Transmetalation of self-assembled, supramolecular complexes. *Chem. Soc. Rev.* **43**, 1825-1834 (2014).
19. Jung, M., Kim, H., Baek, K., Kim, K. Synthetic ion channel based on metal–organic polyhedra. *Angew. Chem. Int. Ed.* **47**, 5755-5757 (2008).
20. Cook, T. R., Stang, P. J. Recent developments in the preparation and chemistry of metallacycles and metallacages *via* coordination. *Chem. Rev.* **115**, 7001-7045 (2015).
21. Sun, Q.-F., *et al.* Self-assembled $M_{24}L_{48}$ polyhedra and their sharp structural switch upon subtle ligand variation. *Science* **328**, 1144-1147 (2010).
22. Beissel, T., Powers, R. E., Parac, T. N., Raymond, K. N. Dynamic isomerization of a supramolecular tetrahedral M_4L_6 cluster. *J. Am. Chem. Soc.* **121**, 4200-4206 (1999).
23. Mahata, K., Frischmann, P. D., Würthner, F. Giant electroactive M_4L_6 tetrahedral host self-assembled with Fe(II) vertices and perylene bisimide dye edges. *J. Am. Chem. Soc.* **135**, 15656-15661 (2013).
24. Custelcean, R., *et al.* Urea-functionalized M_4L_6 cage receptors: anion-templated self-assembly and selective guest exchange in aqueous solutions. *J. Am. Chem. Soc.* **134**, 8525-8534 (2012).
25. Loffler, S., *et al.* Internal dynamics and guest binding of a sterically overcrowded host. *Chem. Sci.* **7**, 4676-4684 (2016).
26. Mecozzi, S., Rebek, J. J. The 55 % solution: a formula for molecular recognition in the liquid state. *Chem. – Eur. J.* **4**, 1016-1022 (1998).
27. García-Simón, C., *et al.* Sponge-like molecular cage for purification of fullerenes. *Nat. Comm.* **5**, 5557 (2014).
28. Kishi, N., Li, Z., Yoza, K., Akita, M., Yoshizawa, M. An M_2L_4 molecular capsule with an anthracene shell: encapsulation of large guests up to 1 nm. *J. Am. Chem. Soc.* **133**, 11438-11441 (2011).
29. Suzuki, K., Takao, K., Sato, S., Fujita, M. Coronene nanophase within coordination spheres: increased solubility of C_{60}. *J. Am. Chem. Soc.* **132**, 2544-2545 (2010).

30. Otte, M., *et al.* Encapsulation of metalloporphyrins in a self-assembled cubic M_8L_6 cage: a new molecular flask for cobalt–porphyrin-catalysed radical-type reactions. *Chem. – Eur. J.* **19**, 10170-10178 (2013).
31. Kubik, S. Molecular cages and capsules with functionalized inner surfaces. In: Albrecht M, Hahn E (eds). *Chemistry of Nanocontainers*. Springer Berlin Heidelberg: Berlin, Heidelberg, 2012, pp 1-34.
32. Wang, W., Wang, Y.-X., Yang, H.-B. Supramolecular transformations within discrete coordination-driven supramolecular architectures. *Chem. Soc. Rev.* **45**, 2656-2693 (2016).
33. Pauling, L. Nature of forces between large molecules of biological interest. *Nature* **161**, 707-709 (1948).
34. Hunter, C. A., Anderson, H. L. What is cooperativity? *Angew. Chem. Int. Ed.* **48**, 7488-7499 (2009).
35. Conway, A., Koshland, D. E. Negative cooperativity in enzyme action. Binding of diphosphopyridine nucleotide to glyceraldehyde-3-phosphate dehydrogenase. *Biochemistry* **7**, 4011-4023 (1968).
36. Mahadevi, A. S., Sastry, G. N. Cooperativity in noncovalent interactions. *Chem. Rev.* **116**, 2775-2825 (2016).
37. Huang, Z., *et al.* Supramolecular chemistry of cucurbiturils: tuning cooperativity with multiple noncovalent interactions from positive to negative. *Langmuir* **32**, 12352-12360 (2016).
38. Badjić, J. D., Nelson, A., Cantrill, S. J., Turnbull, W. B., Stoddart, J. F. Multivalency and cooperativity in supramolecular chemistry. *Acc. Chem. Res.* **38**, 723-732 (2005).
39. Rebek, J., *et al.* Allosteric effects in organic chemistry: binding cooperativity in a model for subunit interactions. *J. Am. Chem. Soc.* **107**, 7481-7487 (1985).
40. Kleywegt, G. J., Jones, T. A. Detection, delineation, measurement and display of cavities in macromolecular structures. *Acta Crystallogr. Sect. D* **50**, 178-185 (1994).
41. Caulder, D. L., Raymond, K. N. Supermolecules by design. *Acc. Chem. Res.* **32**, 975-982 (1999).
42. Bell, Z. R., Jeffery, J. C., McCleverty, J. A., Ward, M. D. Assembly of a truncated-tetrahedral chiral $[M_{12}(\mu\text{-}L)_{18}]^{24+}$ cage. *Angew. Chem. Int. Ed.* **41**, 2515-2518 (2002).
43. Ghosh, K., Hu, J., White, H. S., Stang, P. J. Construction of multifunctional cuboctahedra *via* coordination-driven self-assembly. *J. Am. Chem. Soc.* **131**, 6695-6697 (2009).
44. Sun, Q.-F., Sato, S., Fujita, M. An $M_{18}L_{24}$ stellated cuboctahedron through post-stellation of an $M_{12}L_{24}$ core. *Nat. Chem.* **4**, 330-333 (2012).
45. Thordarson, P. Determining association constants from titration experiments in supramolecular chemistry. *Chem. Soc. Rev.* **40**, 1305-1323 (2011).
46. Bindfit v0.5. http://app.supramolecular.org/bindfit/ (accessed January-June 2016).
47. Snyder, D. A., *et al.* Comparisons of NMR spectral quality and success in crystallization demonstrate that NMR and X-ray crystallography are complementary methods for small protein structure determination. *J. Am. Chem. Soc.* **127**, 16505-16511 (2005).
48. Guldi, D. M. Molecular porphyrinfullerene architectures. *Pure Appl. Chem.* **75**, 1069-1075 (2003).
49. Burke, M. J., Nichol, G. S., Lusby, P. J. Orthogonal selection and fixing of coordination self-assembly pathways for robust metallo-organic ensemble construction. *J. Am. Chem. Soc.* **138**, 9308-9315 (2016).